

Excitonic absorption spectra of metallic single-walled carbon nanotubes

Ermin Malic,^{1,*} Janina Maultzsch,² Stephanie Reich,³ and Andreas Knorr¹

¹*Institut für Theoretische Physik, Nichtlineare Optik und Quantenelektronik von Halbleitern, Technische Universität Berlin, 10623 Berlin, Germany*

²*Institut für Festkörperphysik, Technische Universität Berlin, 10623 Berlin, Germany*

³*Fachbereich Physik, Freie Universität Berlin, 14195 Berlin, Germany*

(Received 3 March 2010; revised manuscript received 22 June 2010; published 22 July 2010)

We present microscopic calculations of the absorption spectra of metallic single-walled carbon nanotubes. We address the controversial question of the excitonic binding energies in metallic nanotubes as well as the excitonic character of higher transitions. In spite of the strong screening, we observe binding energies in the range of 100 meV for metallic nanotubes with diameters in the range of 1–2.2 nm. Characteristic features of the absorption spectra, such as peak splitting and an asymmetric peak shape, are observed. The splitting is due to the trigonal warping effect. The peak shoulder at high energies is a result of an overlap of the excitonic excitation with the free-particle Van Hove singularity. Furthermore, we find higher transitions to be also significantly influenced by excitons. Our approach is based on density matrix, which allows the investigation of the chirality and diameter dependence of the excitonic binding energy for the first four optical transitions for a variety of different metallic and semiconducting nanotubes.

DOI: [10.1103/PhysRevB.82.035433](https://doi.org/10.1103/PhysRevB.82.035433)

PACS number(s): 78.67.Ch, 73.22.-f, 78.47.-p

Single-walled carbon nanotubes (CNTs) are tiny hollow cylinders constructed by rolling up graphene. They are prototypical one-dimensional structures, since their diameter is in the range of one nanometer, whereas their length can reach several micrometers.^{1,2} Depending on the rolling angle, a variety of nanotubes with different physical properties can be created. The microscopic structure of CNTs is uniquely described by their diameter d and their chiral angle ϕ , which are fully determined by the chiral indices (n_1, n_2) . Nanotubes can be classified in three different families:¹ (i) metallic, (ii) +1 semiconducting, and (iii) -1 semiconducting tubes, cf. Fig. 1. As a result, one third of all possible CNT configurations is metallic, i.e., two subbands cross at the Fermi level. Due to their unique physical properties, CNTs are promising candidates for applications in nanoscale electronic devices, such as transistors, emitters, and detectors.²

For a long time, the optical excitations in CNTs were believed to be completely understood within the one-particle picture. However, many-body *ab initio* calculations^{3–7} predicted the excitonic character of optical excitations in semiconducting nanotubes. In 2005, two-photon absorption experiments confirmed the crucial role of excitons for CNTs.^{8,9} So far, only few theoretical studies on the optical properties of metallic CNTs^{3,10,11} have been performed revealing that surprisingly excitonic effects significantly change the optical properties of metallic CNTs. However, there is a controversial discussion about the value of the excitonic binding energy, Deslippe *et al.*¹⁰ performed *ab initio* calculations based on the GW-Bethe-Salpeter equation (GW-BSE) technique finding excitonic binding energies in metallic nanotubes to be around 50 meV, which is one order of magnitude smaller than in semiconducting tubes of comparable diameter. In contrast, Wang *et al.*¹¹ applying the Pariser-Parr-Pople (PPP) model claim that metallic CNTs exhibit optical behavior very similar to comparable semiconducting tubes. They predict excitonic binding energies in the range of 300 meV.

In this work, we present microscopic calculations of the absorption coefficient $\alpha(\omega)$ for a large number of different

carbon nanotubes. We address the controversial questions of (i) excitonic binding energies of metallic CNTs and (ii) the excitonic character of higher transitions in metallic and semiconducting CNTs. Our approach is based on density matrix theory.^{13–17} In combination with zone-folded tight-binding wave function, it allows the investigation of CNTs of arbitrary chiral angle and over a wide range of diameters, which is an advantage over *ab initio* theories being restricted to small nanotubes. We illustrate the strength of the theory by performing microscopic calculations on the chirality and the diameter dependence of excitonic absorption spectra of all three nanotube families. We expect our theory to be similar as the Bethe Salpeter approach^{10,18} within the Hartree Fock level. However, the potential of the density matrix theory lies in the study of Coulomb- and phonon-induced relaxation dy-

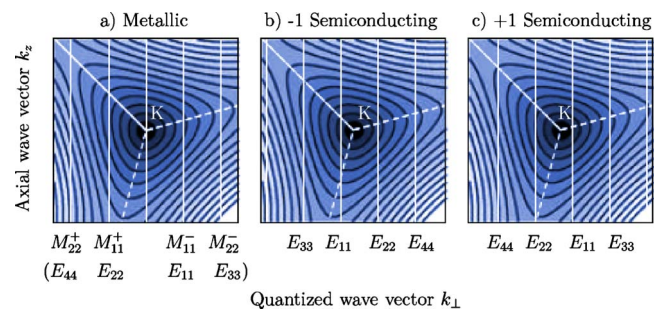


FIG. 1. (Color online) Energy contour of graphene. Due to the boundary condition around the nanotube circumference, the wave vector decouples in a continuous component k_z along the tube axis and a quantized perpendicular component $k_\perp = \frac{2}{d}m$ with the diameter d and the subband index m . The solid white lines correspond to lowest subbands E_{ii} in the three nanotube families: (a) metallic tubes [if $(n_1 - n_2) \bmod 3 = 0$] with a line containing the K point, (b) -1 semiconducting tubes [if $(n_1 - n_2) \bmod 3 = -1$], and (c) +1 semiconducting tubes [if $(n_1 - n_2) \bmod 3 = +1$]. The semiconducting families differ in the position of the lowest transition E_{11} with respect to the K point. After Ref. 12.

namics of nonequilibrium charge carriers. It allows a microscopic access to their time and momentum-resolved scattering dynamics.^{15,19,20}

In the presence of an optical field, the material responds by forming a microscopic dipole density resulting in a polarization $\mathbf{P}(\mathbf{r}, t)$ of the material. In linear and homogeneous materials, the polarization and the optical field are parallel²¹

$$\mathbf{P}(\omega) = \varepsilon_0 \chi(\omega) \mathbf{E}(\omega). \quad (1)$$

The proportionality coefficient is given by the optical susceptibility $\chi(\omega) = \varepsilon(\omega) - 1$ describing the linear response of the system to a perturbation in a spatially homogeneous system. The intensity $I(z)$ of an electromagnetic wave propagating in z direction is given by $I(z) = |E(z)|^2 = e^{-\alpha(\omega)z}$ with the absorption coefficient²¹

$$\alpha(\omega) = \frac{\omega}{cn(\omega)} \text{Im} \chi(\omega), \quad (2)$$

describing the propagation depth of light in the material. The calculation of $\alpha(\omega)$ requires the knowledge of the optical susceptibility $\chi(\omega)$, which is determined as the ratio between the macroscopic polarization and the optical field, cf. Eq. (1).

The macroscopic polarization $\mathbf{P}(t)$ is determined by the coherence $p_k(t)$, which is a measure for the transition probability between the conduction and the valence band at the wave vector k . The latter can be calculated within the formalism of density matrix theory yielding the CNT Bloch equation^{16,20,21}

$$\dot{p}_k(t) = -i\tilde{\omega}_k p_k(t) + i\tilde{\Omega}_k(t) - \gamma p_k(t). \quad (3)$$

The equation describes the linear response, i.e., it is assumed that the driving field is small resulting in a negligible change of occupation probabilities.²¹ The parameter³ $\gamma = (0.0125/\hbar)$ eV accounts for dephasing processes, which determine the line width of the optical transition.

The oscillator strength and the transition energy are determined microscopically by the Rabi frequency $\tilde{\Omega}_k(t) = \frac{e_0}{m_0} M_z^{cv}(\mathbf{k}) A(t) - \frac{1}{\hbar} \sum_{k'} W_{e-h}(k, k') p_{k'}(t)$ and the band gap energy $\tilde{\omega}_k = (\omega_c(k) - \omega_v(k)) - \frac{1}{\hbar} \sum_{k'} W_{e-e}(k, k')$, respectively. For the optical matrix element $M_z^{cv}(\mathbf{k})$ we obtain a fully analytical expression for the optical matrix element $M_z^{cv}(\mathbf{k})$ for light polarized along the nanotube axis^{14,22,23} within the tight-binding model.

The Coulomb interaction is considered within the screened Hartree-Fock level. We take into account both the Hartree and the Fock terms leading to (i) the renormalization of the band-gap due to the repulsive electron-electron interaction^{16,24} $W_{e-e}(k, k') = W_{v_k, v_{k'}}^{v_{k'}, v_k} - W_{v_{k'}, c_k}^{c_k, v_{k'}}$ (corresponding to the self-energy correction) and (ii) the renormalization of the Rabi frequency due to the attractive electron-hole interaction $W_{e-h}(k, k') = W_{c_k', v_k}^{c_k, v_{k'}} - W_{v_k, c_k'}^{c_k', v_k}$. The screened Coulomb matrix elements $W_{v_k, v_{k'}}^{v_{k'}, v_k}$ are defined and discussed below. While (i) accounts for a considerable blue shift of the free-particle Van Hove singularities, (ii) is responsible for the formation of bound electron-hole pairs leading to redshifted excitonic Lorentz peaks in the absorption spectra.^{16,20,24}

The bare Coulomb matrix elements are given by

$$V_{l_3, l_4}^{l_1, l_2} = \int \int d\mathbf{r} d\mathbf{r}' \Phi_{l_1}^*(\mathbf{r}) \Phi_{l_2}^*(\mathbf{r}') V_{Coul}(\mathbf{r} - \mathbf{r}') \Phi_{l_3}(\mathbf{r}') \Phi_{l_4}(\mathbf{r}),$$

where $V_{Coul}(\mathbf{r} - \mathbf{r}')$ is the Coulomb potential and l_i are compound indices containing the wave vector k and the band index $\lambda = c, v$. The wave functions $\Phi_{l_i}(\mathbf{r})$ are expressed within the tight-binding approximation.²⁵ The Coulomb interaction is parametrized by the Ohno potential, which has already been shown to be a good approximation for CNTs.^{6,18,24} More details can be found in Ref. 24.

Since we are, in particular, interested in describing optical properties of metallic CNTs, screening of the Coulomb interaction plays an important role.²¹ $W_{l_3, l_4}^{l_1, l_2}(q) = V_{l_3, l_4}^{l_1, l_2}(q) / [\varepsilon_{bg} \varepsilon(q)]$ with dielectric function $\varepsilon(q)$ depending on the momentum transfer q , and the dielectric background constant ε_{bg} . The latter describes the influence of the environment created by solvents and adsorbed molecules, which have a considerable influence on optical properties of carbon nanotube.^{18,26} In this work, however, the focus lies on the investigation of the internal screening denoted by $\varepsilon(q)$. Therefore, we describe CNTs in air or vacuum with a fixed $\varepsilon_{bg} = 1$. The dielectric function $\varepsilon(q)$ is calculated within the static limit of the Lindhard approximation^{18,21}

$$\varepsilon(q) = 1 - 2V(q) \sum_{k, \lambda, \lambda'} \frac{\rho_{k-q}^{\lambda'} - \rho_k^{\lambda}}{E_{k-q}^{\lambda'} - E_k^{\lambda}} \left| \int d\mathbf{r} \Phi_{k, \lambda}^* e^{-iqr} \Phi_{k-q, \lambda'} \right|^2 \quad (4)$$

with the band index $\lambda = c, v$, the occupation probabilities $\rho_k^{\lambda} = \langle a_{\lambda k}^{\dagger} a_{\lambda k} \rangle$, which are evaluated within the limit of linear optics, and with the single-particle energies E_k^{λ} .

Figure 2 illustrates $\varepsilon(q)$ as a function of the momentum transfer q for an exemplary CNT of each family (see Fig. 1). The striking difference is the diverging dielectric function for metallic tubes in the limit of small q . In contrast, for semiconducting tubes, $\varepsilon(q)$ takes the value 1 for $q=0$, since $\lim_{q \rightarrow 0} \left| \int d\mathbf{r} \Phi_{k, \lambda}^* e^{-iqr} \Phi_{k-q, \lambda'} \right|^2 = 0$. This means that the influence of screening vanishes for semiconducting tubes for processes with a small momentum transfer q . The difference between the two different semiconducting families is negligibly small. Furthermore, in the limit of large q , the dielectric function goes toward the value 1 for all CNTs reflecting the decreasing Coulomb matrix elements for a large momentum transfer.²⁴

In spite of the strong screening in metallic CNTs, the calculation of the absorption coefficient according to Eq. (2) reveals that excitonic effects have a crucial influence on their optical properties. Figure 3 shows absorption spectra for metallic tubes along an exemplary Kataura branch¹ with $2n_1 + n_2 = 27$. These tubes are characterized by a roughly constant diameter $d \approx 1$ nm. The spectra exhibit double-peaked structures arising from the trigonal warping effect, which describes the deviation of the equienergy contour from a circle around the K point in the Brillouin zone.²⁷⁻²⁹ The corresponding peak splitting increases for small chiral angles and high transition energies. Furthermore, the peaks show an interesting shape exhibiting a strong Lorentz-like contribution, which reflects the excitonic character of optical excitations.

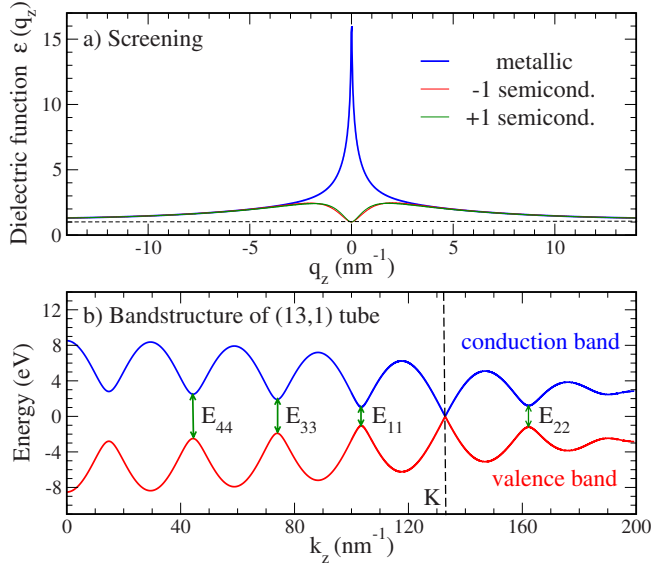


FIG. 2. (Color online) (a) The dielectric function $\epsilon(q)$, which describes the internal screening, is shown for the exemplary metallic (13,1), the -1 semiconducting (12,1), and +1 semiconducting (14,1) nanotube. The figure illustrates that the screening in metallic tubes plays a crucial role. While the dielectric function $\epsilon(q)$ for both semiconducting CNTs goes to the value 1 for a small momentum transfer q , it diverges for the metallic tube. (b) Band structure of the (13,1) tube with optical transitions E_{ii} leading to pronounced peaks in the absorption spectrum, cf. Fig. 3. Note, that the overlap parameter s_0 has been neglected leading to a symmetry between the valence and the conduction band.

The long shoulder on the high-energy side, on the other hand, is typical for free-particle Van Hove singularities. The explanation is found by comparing absorption spectra of metallic and semiconducting CNTs, see Fig. 4. The exemplary metallic (13,1) tube with $d \approx 1$ nm and $\phi = 3.7^\circ$ is compared with the semiconducting (14,1) and (12,1) CNTs, which have been chosen since they have a similar diameter and a similar chiral angle. By switching off the attractive electron-hole contribution $W_{e-h}(k, k')$ in Eq. (3) (dashed lines in Fig. 4), we can easily determine the influence of excitons (bound electron-hole pairs) on the absorption spectra. The excitonic binding energy $E_{b,ii}$ is given as the energetical difference between the solid-line peak, which contains the electron-hole interaction $W_{e-h}(k, k')$ and the corresponding dashed-line peak without $W_{e-h}(k, k')$. For the metallic (13,1) CNT, we find $E_{b,11} = 78$ meV and $E_{b,22} = 114$ meV, which is unexpectedly large for a metallic structure. The value is clearly higher than the thermal energy of 25 meV at room temperature. Hence, excitonic character of transition can even be measured.³⁰

The reason for the appearance of bound electron-hole states in metallic tubes lies in an ineffective screening in one-dimensional systems compared to bulk metals, where excitonic effects are of minor importance. Nevertheless, the screening is still much stronger than for semiconducting nanotubes, which explains the smaller excitonic binding energy and the reduced transfer of oscillator strength from the free particle to excitonic peaks. As a consequence, there is an

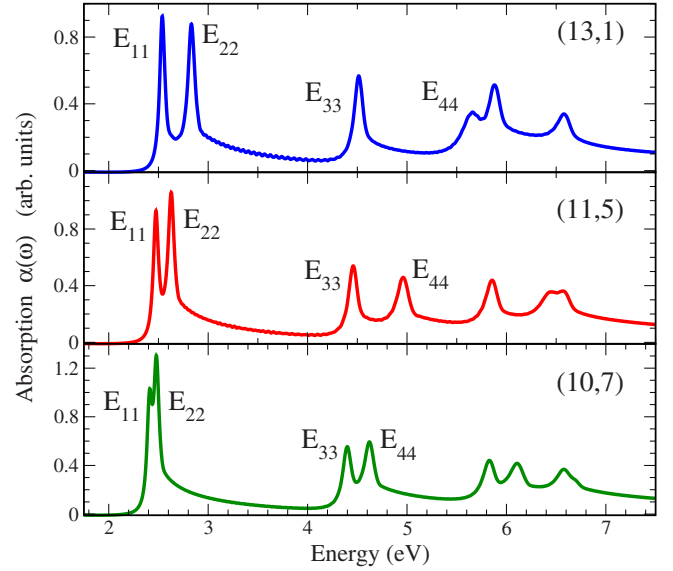


FIG. 3. (Color online) Absorption coefficient $\alpha(\omega)$ including excitonic effects, cf. Eq. (2), as a function of the energy for three metallic tubes, which are located along the Kataura branch (Ref. 12) with $2n_1 + n_2 = 27$. The chiral angle increases from top to bottom, while the diameter has a nearly constant value of about 1 nm. The figure illustrates a double-peaked structure originating from the trigonal warping effect. For an easier comparison with semiconducting CNTs, the peaks are denoted by E_{11} , E_{22} , E_{33} , and E_{44} . This corresponds to the notation $M_{11}^-, M_{11}^+, M_{22}^-, M_{22}^+$, which is often used in literature (Ref. 27), cf. Fig. 1.

overlap between the symmetric excitonic Lorentzians and (renormalized) free-particle Van Hove singularities leading to the observed high-energy shoulder, see Fig. 4(a). This characteristic peak shape has been reported¹⁰ and confirmed experimentally.³⁰ For comparison, the spectra of semiconducting tubes are entirely characterized by excitonic peaks, see Figs. 4(b) and 4(c). The excitonic binding energies are considerably larger than in metallic CNTs: for the -1 semiconducting (12,1) CNT we find $E_{b,11} = 460$ meV and $E_{b,22} = 491$ meV and for the +1 semiconducting (14,1) CNT $E_{b,11} = 377$ meV and $E_{b,22} = 474$ meV. Here, the oscillator strength is almost completely transferred to excitons. The free-particle continuum does not have any measurable influence on the peak shape. In contrast to metallic tubes, higher excitonic states (corresponding to the Rydberg series in the hydrogen atom) with a relatively small intensity can be found in the absorption spectra of semiconducting CNTs, see Figs. 4(b) and 4(c). Their absence in metallic CNTs is probably due to the weak excitonic oscillator strength with respect to semiconducting nanotubes.

In Figs. 5 and 6, we systematically investigate the chiral and diameter dependence of the excitonic binding energy $E_{b,ii}$ for the first four transitions in the spectra of metallic, -1, and +1 semiconducting CNTs, respectively. Both figures show the importance of excitonic effects for metallic CNTs. They also illustrate that their excitonic binding energies are considerably smaller than for semiconducting tubes of comparable diameter. Furthermore, all four transitions are characterized by excitons—a point that has been controversially

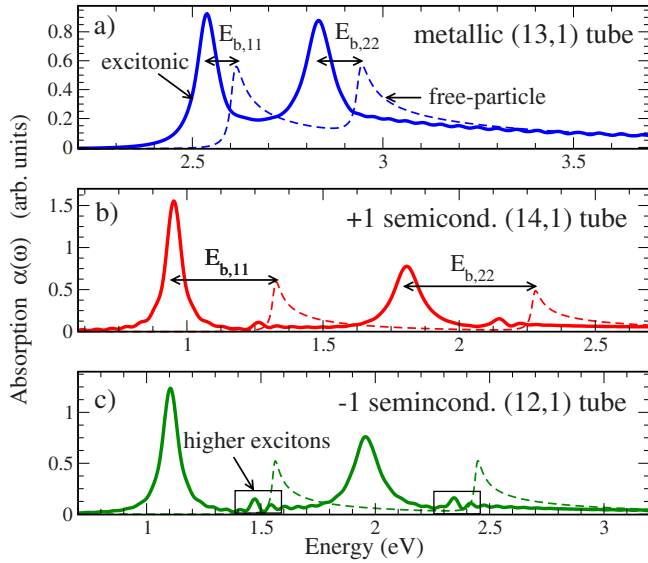


FIG. 4. (Color online) A zoom of the first two transitions in the absorption spectra of (a) the metallic (13,1), (b) +1 semiconducting (14,1), and (c) -1 semiconducting (12,1) tube is shown. The solid lines exhibit the absorption coefficient including the full Coulomb interaction. The dashed lines correspond to calculations, where the attractive electron-hole interaction $W_{e-h}(k, k')$ has been switched off [note that the electron-electron interaction $W_{e-e}(k, k')$ is still included, cf. Eq. (3)]. The arrows in (b) illustrate the excitonic binding energies $E_{b,ii}$. The boxes in (c) show higher excitonic states appearing only in the spectra of semiconducting CNTs.

discussed in literature.^{31,32} We obtain excitonic binding energies in the range of about 500 meV for semiconducting nanotubes with $d \sim 1$ nm, which is in good agreement with other theoretical results.^{4,5,18} Including a realistic dielectric background screening constant of $\epsilon_{bg} \approx 2$, which describes the

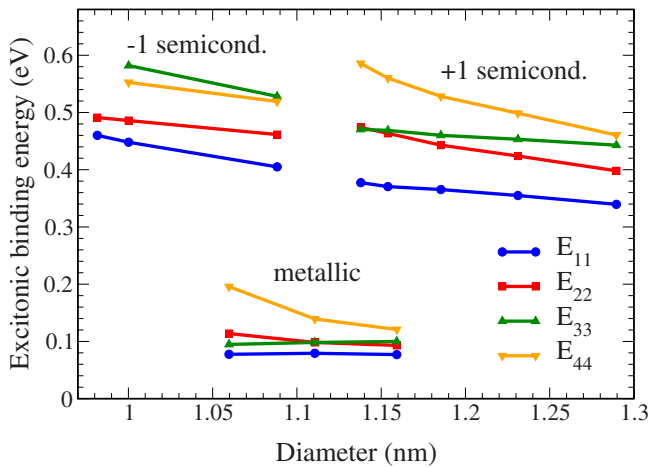


FIG. 5. (Color online) Chirality dependence: Excitonic binding energy $E_{b,ii}$ for the first four transitions of metallic, -1, and +1 semiconducting tubes along the Kataura branches (Ref. 12) with $2n_1 + n_2 = 27, 25$, and 29, respectively. Since these tubes have a similar diameter, the plot shows the dependence of $E_{b,ii}$ on the chiral angle, which increases from left to right in the range of $3^\circ - 28^\circ$. The figure also illustrates the smaller binding energies for metallic CNTs.

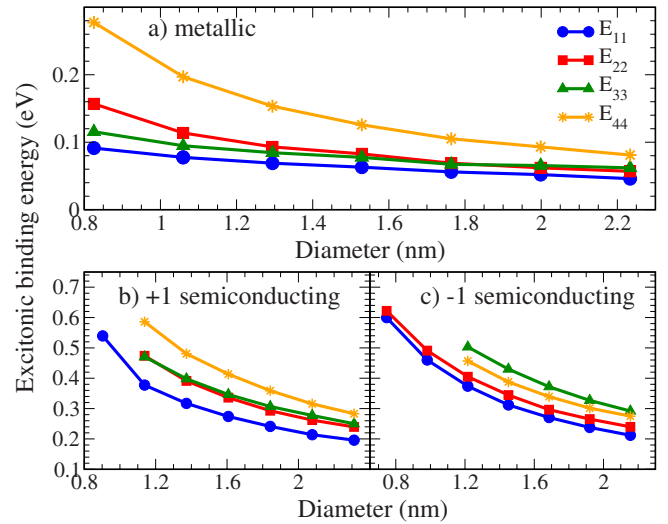


FIG. 6. (Color online) Diameter dependence: Excitonic binding energy $E_{b,ii}$ for the first four transitions are shown over a wide diameter range exhibiting a $1/d$ dependence for both metallic and semiconducting tubes. For higher transitions, in some cases it is difficult to determine the binding energy due to the overlap of different peaks.

influence of the surrounding medium, the binding energy is reduced²⁶ to approximately 300 meV, which is in good agreement with the experimental finding.^{8,9} For metallic nanotubes, we obtain smaller excitonic binding energies in the range of about 100 meV. This agrees well with the theoretical results in Refs. 3 and 10, and experimental findings reported in Ref. 30.

In Fig. 5, we find the chirality dependence to be weak: CNTs with small chiral angle tend to have larger $E_{b,ii}$. For metallic nanotubes, the first three transitions are nearly constant, only the highest transition E_{44} shows a clear chirality dependence. In the case of semiconducting tubes, the increase is observed to be slightly stronger for E_{22} and E_{44} (E_{11} and E_{33}) for +1(-1) tubes. These transitions have in common, that they lie on the same high-symmetry line in the Brillouin zone, see Figs. 1(b) and 1(c). In our earlier work, they have already been reported to show stronger absorption.^{14,33} Figure 6 exhibits the behavior of excitonic binding energies over a wide range of diameters (for a nearly constant chiral angle of $2^\circ - 3^\circ$). Note, that for nanotubes with diameters below 1 nm hybridization effects might play an important role.³⁴ Here, the zone-folded tight-binding wave functions can be inappropriate. For our investigations, we have included just one nanotube below 1 nm for comparison and we find that its excitonic binding energy does not deviate from the behavior of larger tubes. Figure 6 reveals a $1/d$ dependence for all four transitions and all nanotube families. Interestingly, $E_{b,22}$ exceeds $E_{b,33}$ for metallic tubes with a small chiral angle. Another interesting feature is found for -1 semiconducting CNTs, where $E_{b,44}$ is surprisingly smaller than $E_{b,33}$, see Fig. 6(c).

In conclusion, we have developed a method to microscopically describe excitonic absorption spectra of carbon nanotubes of arbitrary chiral angle and over a wide range of diameters. Our approach is based on density matrix theory

combined with zone-folded tight-binding wave functions. We find excitonic effects to crucially influence the optical properties of both semiconducting and metallic tubes. The excitonic binding energies for metallic CNTs with $E_b \approx 100$ meV are much larger than for metallic bulk structures. However, they are still considerably smaller than for comparable semiconducting nanotubes. We have presented a systematic study on chirality and diameter dependence of the

excitonic binding energy for the lowest four transitions. We show that even higher transitions are significantly influenced by excitons. The gained insights can be helpful for an unambiguous identification of carbon nanotubes.

We acknowledge the support from Sfb 658 and the ERC under Grant No. 210642.

*ermin.malic@tu-berlin.de

- ¹S. Reich, C. Thomsen, and J. Maultzsch, *Carbon Nanotubes: Basic Concepts and Physical Properties* (Wiley-VCH, Berlin, 2004).
- ²A. Jorio, M. Dresselhaus, and G. Dresselhaus, *Carbon Nanotubes: Advanced Topics in the Synthesis, Structure, Properties and Applications* (Springer, New York, 2008).
- ³C. D. Spataru, S. Ismail-Beigi, L. X. Benedict, and S. G. Louie, *Phys. Rev. Lett.* **92**, 077402 (2004).
- ⁴V. Perebeinos, J. Tersoff, and P. Avouris, *Phys. Rev. Lett.* **92**, 257402 (2004).
- ⁵E. Chang, G. Bussi, A. Ruini, and E. Molinari, *Phys. Rev. B* **72**, 195423 (2005).
- ⁶H. Zhao and S. Mazumdar, *Phys. Rev. Lett.* **93**, 157402 (2004).
- ⁷V. Perebeinos, J. Tersoff, and P. Avouris, *Nano Lett.* **5**, 2495 (2005).
- ⁸F. Wang, G. Dukovic, L. E. Brus, and T. F. Heinz, *Science* **308**, 838 (2005).
- ⁹J. Maultzsch, R. Pomraenke, S. Reich, E. Chang, D. Prezzi, A. Ruini, E. Molinari, M. S. Strano, C. Thomsen, and C. Lienau, *Phys. Rev. B* **72**, 241402(R) (2005).
- ¹⁰J. Deslippe, C. D. Spataru, D. Prendergast, and S. G. Louie, *Nano Lett.* **7**, 1626 (2007).
- ¹¹Z. Wang, D. Psiachos, R. F. Badilla, and S. Mazumdar, *J. Phys.: Condens. Matter* **21**, 095009 (2009).
- ¹²C. Thomsen and S. Reich, in *Raman Scattering in Carbon Nanotubes in Light Scattering in Solids IX*, edited by M. Cardona and R. Merlin (Springer, Berlin, 2007).
- ¹³F. Rossi and T. Kuhn, *Rev. Mod. Phys.* **74**, 895 (2002).
- ¹⁴E. Malić, M. Hirtschulz, F. Milde, A. Knorr, and S. Reich, *Phys. Rev. B* **74**, 195431 (2006).
- ¹⁵S. Butscher, F. Milde, M. Hirtschulz, E. Malić, and A. Knorr, *Appl. Phys. Lett.* **91**, 203103 (2007).
- ¹⁶M. Hirtschulz, F. Milde, E. Malić, S. Butscher, C. Thomsen, S. Reich, and A. Knorr, *Phys. Rev. B* **77**, 035403 (2008).
- ¹⁷M. Kira and S. Koch, *Prog. Quantum Electron.* **30**, 155 (2006).
- ¹⁸J. Jiang, R. Saito, G. G. Samsonidze, A. Jorio, S. G. Chou, G. Dresselhaus, and M. S. Dresselhaus, *Phys. Rev. B* **75**, 035407 (2007).
- ¹⁹M. Hirtschulz, E. Malic, F. Milde, and A. Knorr, *Phys. Rev. B* **80**, 085405 (2009).
- ²⁰E. Malić, M. Hirtschulz, S. Reich, and A. Knorr, *Phys. Status Solidi (RRL)* **3**, 196 (2009).
- ²¹H. Haug and S. W. Koch, *Quantum Theory of the Optical and Electronic Properties of Semiconductors* (World Scientific, Singapore, 2004).
- ²²A. Grüneis, R. Saito, G. G. Samsonidze, T. Kimura, M. A. Pimenta, A. Jorio, A. G. Souza Filho, G. Dresselhaus, and M. S. Dresselhaus, *Phys. Rev. B* **67**, 165402 (2003).
- ²³A. Zarifi and T. G. Pedersen, *J. Phys.: Condens. Matter* **20**, 275211 (2008).
- ²⁴E. Malić, M. Hirtschulz, F. Milde, J. Maultzsch, S. Reich, and A. Knorr, *Phys. Status Solidi B* **245**, 2155 (2008).
- ²⁵S. Reich, J. Maultzsch, C. Thomsen, and P. Ordejón, *Phys. Rev. B* **66**, 035412 (2002).
- ²⁶E. Malić, M. Hirtschulz, J. Maultzsch, S. Reich, and A. Knorr, *Phys. Status Solidi B* **246**, 2592 (2009).
- ²⁷E. Malić, M. Hirtschulz, F. Milde, Y. Wu, J. Maultzsch, T. F. Heinz, A. Knorr, and S. Reich, *Phys. Rev. B* **77**, 045432 (2008).
- ²⁸R. Saito, G. Dresselhaus, and M. S. Dresselhaus, *Phys. Rev. B* **61**, 2981 (2000).
- ²⁹S. Reich and C. Thomsen, *Phys. Rev. B* **62**, 4273 (2000).
- ³⁰F. Wang, D. J. Cho, B. Kessler, J. Deslippe, P. J. Schuck, S. G. Louie, A. Zettl, T. F. Heinz, and Y. R. Shen, *Phys. Rev. Lett.* **99**, 227401 (2007).
- ³¹P. T. Araujo, S. K. Doorn, S. Kilina, S. Tretiak, E. Einarsson, S. Maruyama, H. Chacham, M. A. Pimenta, and A. Jorio, *Phys. Rev. Lett.* **98**, 067401 (2007).
- ³²T. Michel, M. Paillet, J. C. Meyer, V. N. Popov, L. Henrard, and J. L. Sauvajol, *Phys. Rev. B* **75**, 155432 (2007).
- ³³E. Malić, M. Hirtschulz, F. Milde, Y. Wu, J. Maultzsch, T. F. Heinz, A. Knorr, and S. Reich, *Phys. Status Solidi B* **244**, 4240 (2007).
- ³⁴X. Blase, L. X. Benedict, E. L. Shirley, and S. G. Louie, *Phys. Rev. Lett.* **72**, 1878 (1994).